J Mater Sci (2009) 44:2945–2956
DOI 10.1007/s10853-009-3391-1

Hold-time effects on elevated-temperature low-cycle-fatigue and crack-propagation behaviors of HAYNES® 188 superalloy

S. Y. Lee · Y. L. Lu · P. K. Liaw · L. J. Chen · S. A. Thompson · J. W. Blust · P. F. Browning · A. K. Bhattacharya · J. M. Aurrecoechea · D. L. Klarstrom

Received: 7 July 2008 / Accepted: 9 March 2009 / Published online: 7 April 2009

Abstract Low-cycle-fatigue (LCF) and fatigue-crack-growth (FCG) behaviors of a cobalt-based HAYNES 188 superalloy were studied at temperatures ranging from 816 to 982 °C in laboratory air. Various tensile-hold times were imposed at the maximum strain and load in the LCF and FCG tests, respectively, to examine the high-temperature fatigue and creep–fatigue interactions. In this article, the effects of hold time and temperature on the cyclic-stress response, fatigue life, fracture mode, and crack-growth rate are discussed. Parameters based on the tensile-hysteresis energy are applied to correlate the LCF lives with and without hold time.

Introduction

HAYNES 188 (39Co–22Ni–22Cr–14W, in weight percent) [1] is a solid-solution-strengthened cobalt-based superalloy that possesses excellent high-temperature strength, ductility, fabricability, weldability, and superior corrosion resistance. It is currently used for a variety of components, such as combustor chambers, transition ducts in commercial aircraft-turbine engines, and afterburner components in the military. These components are usually used in situations where low-cycle-fatigue (LCF), creep, and their combinations are the main damage mechanisms that limit service lifetimes. Thus, it is of importance to investigate the elevated-temperature LCF and fatigue-crack-growth (FCG) behaviors of the HAYNES 188 alloy with and without hold time for designing high-temperature components safely and finding the potential usage of the alloy.

The fatigue lifetime depends not only on the temperature but also on the loading waveform due to the creep damage. Generally, the lifetimes are decreased by the increase of the temperature [2–4], and the damage is caused by a combination of fatigue and creep mechanisms [5–9]. Various strain-hold tests have been extensively performed to investigate the creep–fatigue interaction behavior for many engineering materials [10–12]. Some studies have examined the elevated-temperature LCF behavior of HAYNES 188 alloy. The effects of the temperature, strain hold, cyclic frequency, and aging treatment on the LCF of HAYNES 188 alloy have been studied [13–18]. However, there are few investigations of the tensile-hold effect on LCF and FCG behaviors.

In the current research, total strain-controlled high-temperature LCF and constant ΔK-controlled FCG experiments were carried out to examine the effects of test temperature and tensile-hold time on the cyclic-stress response behavior, LCF lifetime, and FCG rate in HAYNES 188 alloy. Fracture surfaces were examined to determine crack initiation and propagation modes. A theoretical method using the tensile-hysteresis energy was

S. Y. Lee · Y. L. Lu · P. K. Liaw (✉) · L. J. Chen
Department of Materials Science and Engineering, The University of Tennessee, 427-B Dougherty Engineering Building, Knoxville, TN 37996-2200, USA
e-mail: pliaw@utk.edu

L. J. Chen
School of Materials Science and Engineering, Shenyang University of Technology, Shenyang 110178, People's Republic of China

S. A. Thompson · J. W. Blust · P. F. Browning · A. K. Bhattacharya · J. M. Aurrecoechea
Solar Turbines, Inc., 2200 Pacific Hwy, PO Box 85376, MZ R-1, San Diego, CA 92186, USA

D. L. Klarstrom
Haynes International, Inc., 1020 W. Park Ave., PO Box 9013, Kokomo, IN 46904, USA

developed to correlate the LCF lives with and without hold time.

Experimental procedures

The HAYNES 188 alloy was supplied by Haynes International, Inc. in a solution-heat-treated condition. The final solution-heat treatment was done at 1175 °C, followed by rapid cooling. The microstructure of the alloy in the as-received condition is shown in Fig. 1. The alloy is mainly composed of austenitic grains with annealing twins. The average grain size was found to be about 45 μm. In addition, a small amount of second-phase particles were observed, which have been determined to be M_6C carbides [19].

The specimen for LCF test was rectangular with a length of 12.8 mm and a width of 6.4 mm in the gauge section, and a thickness of 3.2 mm, as shown in Fig. 2a. All fully reversed, pull-push, LCF tests with and without hold times were performed in laboratory air employing a computer-controlled servo-hydraulic material test system (MTS). A resistance furnace was employed to heat the specimens. The fluctuation of the test temperature along the gauge section of the specimen is maintained at least within a range of ±2 °C. An axial total strain-range control mode was applied. In this article, only uniaxial loading case is concerned. A high-temperature extensometer was employed to monitor the axial strain. The extensometer was spring-loaded and had two ceramic legs, which were in direct contact with the gauge-length area of the specimen. LCF tests without hold time were performed with a strain ratio, R, of -1 ($R = \varepsilon_{min}/\varepsilon_{max}$, where ε_{min} and ε_{max} are the applied minimum and maximum strains, respectively) and a cyclic frequency of 1 Hz. The imposed axial total strain ranges were 0.4%, 0.5%, 0.7%, 1.0%, 1.2%, and 2.0%. The test temperatures were 816, 871, 927, and 982 °C, which will cover the application temperatures of the alloy. For LCF tests with hold times, a hold time of 2, 10, or 60 min was introduced at the maximum tensile strain of each cycle. All tests were run to failure, i.e., to the final separation of the specimen.

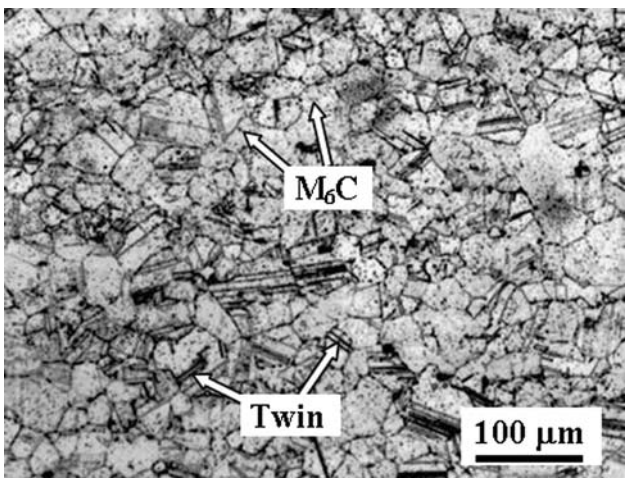

Fig. 1 The microstructure of the as-received HAYNES 188 alloy

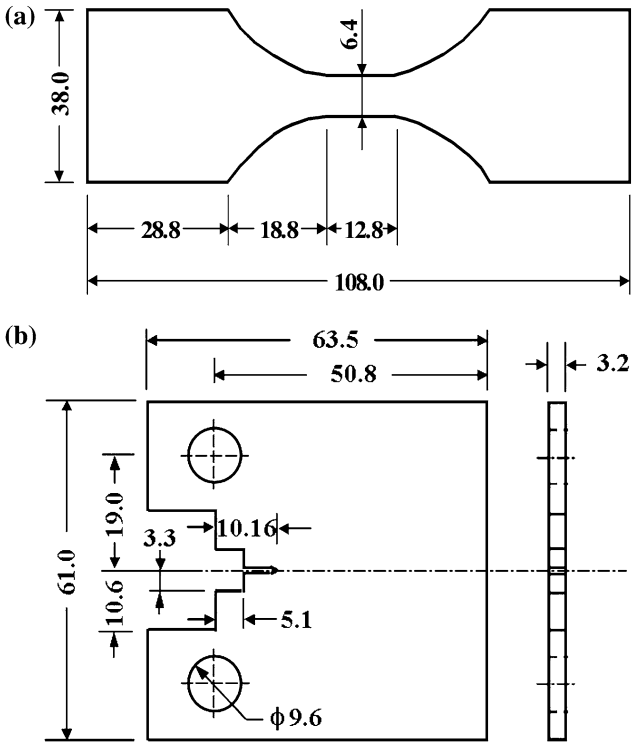

Fig. 2 The sample geometry used for **a** Low-cycle-fatigue and **b** fatigue-crack-growth tests (unit: mm)

The FCG experiments were performed on a compact-tension (CT) specimen prepared according to the American Society for Testing and Materials (ASTM) Standards E647-99 [20]. The specimen has a notch length of 10.16 mm, a width of 50.8 mm, and a thickness of 3.2 mm, as shown in Fig. 2b. Crack-growth tests were conducted using an Instron servo-controlled, hydraulically actuated, and closed-loop test machine. The fluctuation of the test temperature was maintained within a range of ±2 °C. A direct-current-potential-drop (DCPD) method was used to measure the crack length. The crack length is related to the electric potential by Johnson's equation [21],

$$\frac{V_m}{V_0} = \frac{\cosh^{-1}\left[\frac{\cosh(\pi y/W)}{\cos(\pi a/W)}\right]}{\cosh^{-1}\left[\frac{\cosh(\pi y/W)}{\cos(\pi a_0/W)}\right]} \quad (1)$$

where V_0 and a_0 are the initial crack-mouth potential and crack length, respectively, V_m and a are the instantaneous crack-mouth potential and crack length, respectively, y is half of the distance between the two points for which the crack-mouth potential is measured, and W is the specimen width. The stress-intensity factor, K, was obtained using the following equation [22]:

$$K = \frac{P(2+\alpha)}{B\sqrt{W}(1-\alpha)^{3/2}} \left(0.886 + 4.64\alpha - 13.32\alpha^2 + 14.72\alpha^3 - 5.6\alpha^4\right) \quad (2)$$

where P = applied load, B = thickness, $\alpha = a/W$, a = crack length, and W = width for a CT specimen.

The FCG tests were carried out at 816 and 927 °C under a constant $\Delta K(= 27.5\ \mathrm{MPa}\sqrt{\mathrm{m}})$ controlled mode in laboratory air. The frequency of triangular waveform was 0.333 Hz with a R-ratio of 0.05 ($R = K_{\min}/K_{\max}$, where $K_{\min}$ and $K_{\max}$ are the minimum and maximum stress-intensity factors, respectively, during a fatigue cycle). Various hold times (e.g., 0, 0.05, 0.167, 0.5, 2, 10, 60, 300 min, and infinite) were introduced at the maximum stress-intensity factor to study the creep–fatigue interactions on the crack-propagation behavior.

A frequency-modified tensile-hysteresis-energy method was used to correlate fatigue lifetimes. Stress-relaxation tests were performed to obtain the hysteresis-energy parameter needed for the fatigue-life predictions with hold time. The samples were elongated with a monotonic tensile strain of 0.5% and then the stress relaxation was monitored as a function of time at 816 and 927 °C. The fracture surfaces of specimens were examined using a LEO scanning electron microscope (SEM) to determine the crack initiation and propagation mechanisms.

Results and discussion

Cyclic-stress response behavior

The cyclic-stress responses are obtained by plotting the tensile peak stresses from the hysteresis loops per cycle. The cyclic-stress responses without hold time in various total strain ranges for both test temperatures of 816 and 927 °C are, respectively, shown in Fig. 3a and b. It can be seen that the cyclic-stress response behavior is dependent on the test temperature and imposed total strain range. At 816 °C, if lower total strain ranges (≤0.7%) are applied, alloy cyclically hardened up to a maximum and saturated until the final drop. At higher total strain ranges (≥1.0%), the alloy showed a softening regime after hardening in the early stage, and stress saturation was not found. At 927 °C, the alloy exhibits a softening regime at all strain levels after hardening in the early stage. Both the cyclic-strain hardening rate and softening rate increased as the total strain range increased.

In Fig. 4, a 2-min-hold time at the maximum tensile strain was applied to study hold-time effects on the cyclic hardening and softening behaviors. The test temperature was 927 °C and the total strain ranges of 0.4%, 1.0%, and 2.0% were applied. Figure 4 contains the same plots as

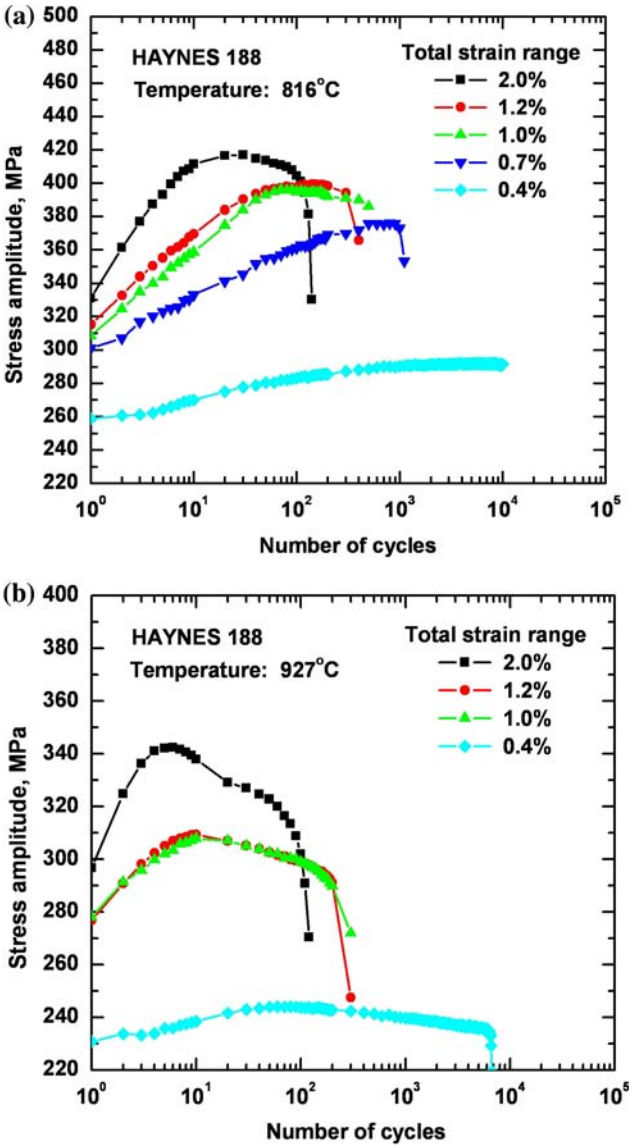

Fig. 3 Cyclic-stress responses at various total strain ranges for the tests without hold time for the HAYNES 188 alloy at **a** 816 °C and **b** 927 °C

Fig. 3b except for stress-response curves of 2-min-hold time at the various strain levels. At lower total strain ranges (≤1.0%), the introduction of hold time decreased the hardening rate and increased the softening rate. For the total strain range of 2.0%, the effect of hold time seemed to be insignificant.

In Fig. 5, the hold time was increased from 2 to 60 min at a fixed total strain range of 1.0%. At 927 °C, the introduction of 2-min-hold time does not change much the initial hardening rate. At about 5 cycles, the stress response changed from hardening to softening. With a 10-min-hold time, softening started at 3 cycles and no hardening region was observed with a 60-min-hold time. As the hold time increased, the softening region started earlier, indicating

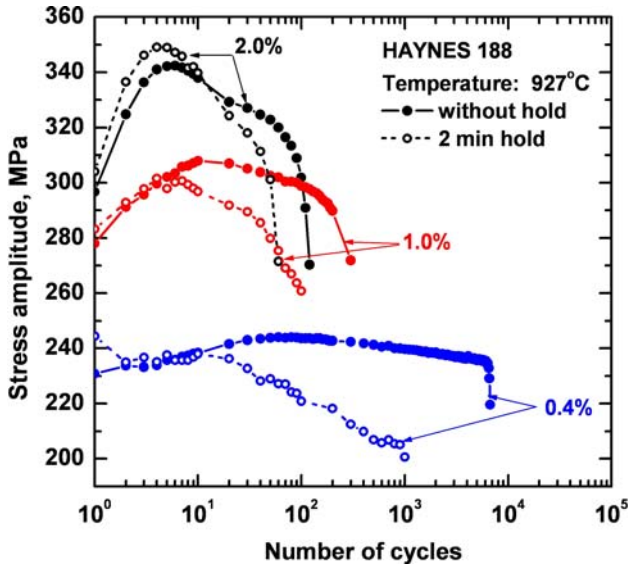

Fig. 4 Effect of 2-min-hold time on the cyclic-stress response for the tests with various total strain ranges at 927 °C

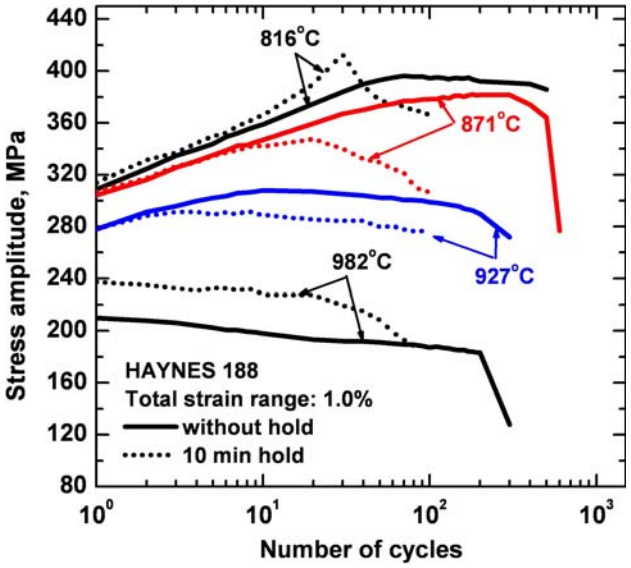

Fig. 6 Effects of temperature and 10-min-hold time on the cyclic-stress response at the total strain range of 1.0%

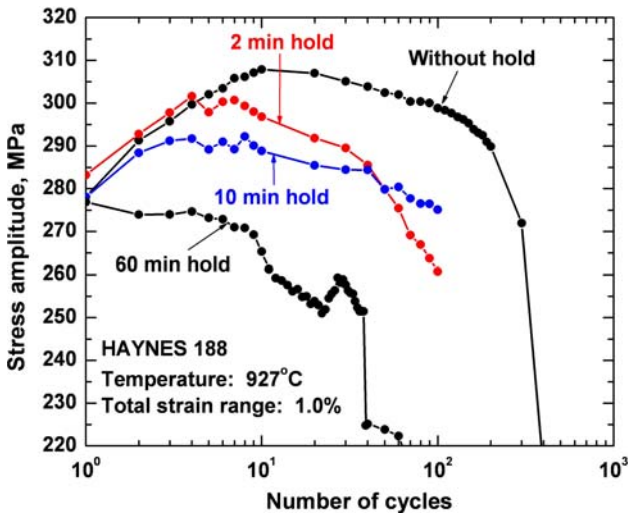

Fig. 5 Effect of hold time on the cyclic-stress response for the test with the total strain range of 1.0% at 927 °C

that the number of cycles needed to reach the maximum stress decreased with increasing the hold time. It was found that the introduction of hold time decreased the fatigue life.

Figure 6 shows the effects of the temperature and 10-min-hold time on the cyclic hardening/softening behavior at the total strain range of 1.0%. The increase of temperature and the introduction of 10-min-hold time generally indicate similar tendencies showing that the hardening rate decreased and the softening rate increased for the cyclic-stress response. When the temperature increases to 982 °C, the alloy exhibits only the cyclic softening. Moreover, the increase of temperature from 816 to 982 °C decreased the stress level with and without hold times.

The hardening behavior during cyclic deformation may be explained by the increase of the dislocation density, dynamic strain aging (DSA), and the interactions of dislocation–dislocation and dislocation–precipitate [15, 23–25]. Rao et al. [15] have extensively studied the LCF behavior of HAYNES 188 alloy over a range of temperature from 25 to 1000 °C using SEM, TEM, and X-ray. In the intermediate temperature range between 300 and 850 °C, they observed that the alloy experienced considerable cyclic hardening and the dislocation substructure progressively changed with increasing temperature. For example, the substructure consisted of dislocation tangles and dipoles at 300 °C, stacking faults, coplanar slip bands, and dislocation pileups in the range 400–600 °C, networks of high dislocation density at 650 °C, and pinning of dislocations by chromium-rich $M_{23}C_6$ at 750 and 850 °C. They pointed out that cyclic hardening can be attributed to the effects of DSA of dislocations by solute atoms at temperature below 700 °C and the combined effect between DSA and precipitation hardening at temperature range between 750 and 850 °C. The multiplication of dislocations and their interactions with diffusing solute atoms and precipitates could lead to the formation of dislocation jogs, pileups, and dislocation pinning, as well as dislocation tangles around carbide precipitates, which would make the mobile dislocations more difficult to glide on the slip plane. Therefore, the cyclic hardening is induced.

On the other hand, the cyclic-softening behavior may be generally ascribed to the dislocation-recovery effects. The recovery of dislocations is known to be not only a thermally activated process but also a dynamic process of the

dislocation annihilation and rearrangement. Higher temperatures and longer hold times are favorable for the recovery of dislocations because longer hold times give sufficient time for dislocations to annihilate and rearrange themselves, and higher temperatures accelerate diffusion rates of atoms. Thus, a dislocation configuration with a lower resistance on the motion of dislocations can be achieved at longer hold time and higher temperature. Furthermore, the development of microcracks formed during fatigue deformation can be thought of as another possible reason for the cycling softening phenomenon, because the formation of crack usually results in the increased compliance of the specimen. In the case that the crack propagation is composed of a large part of the fatigue life at high temperature, the compliance of the specimen is increasing throughout the test and the stress response will decrease in magnitude. At large strain range of 2.0% shown in Fig. 3, the stress amplitude drop-off is very steep after the initial cyclic hardening behavior, which suggests that the drop-off could be due to cracking.

Fatigue-life behavior

Figure 7 shows the effects of 2-min-hold time and total strain range on the fatigue life at 816 °C (Fig. 7a) and 927 °C (Fig. 7b), respectively. The fatigue life is defined as the number of cycles to failure or specimen rupture. Generally, as the total strain range increased, the fatigue life decreased. The introduction of 2-min-hold time apparently resulted in the considerable decrease of the fatigue life at both 816 and 927 °C for all the total strain ranges. The influences of temperature and 10-min-hold time on the LCF life at a total strain range of 1% is presented in Fig. 8. It was found that the fatigue life decreased with increasing the test temperature and the fatigue-life reduction was significant when the 10-min-hold time was introduced.

The fatigue-life fraction as a function of hold time for the total strain range of 1% is shown in Fig. 9. The fatigue-life fraction is defined as a ratio of cycles to failure for the fatigue tests with the hold time (N_f^H) to those for the continuous fatigue tests (N_f^C). At both test temperatures, the fatigue life decreases as the hold time increases. Especially, it is noted that the fatigue life of the test with 2-min-hold time showed approximately a half life, as compared to the test without hold time. Consequently, the introduction of hold time resulted in a considerable decrease on the LCF life.

The fatigue-life reduction with the increase of either the test temperature or tensile-strain hold time could be explained by time-dependent damage, such as creep and oxidation. The introduction of hold time at the maximum tensile strain develops a creep strain component accompanying the stress relaxation in the total strain-controlled LCF test. If creep is predominant deformation mechanism

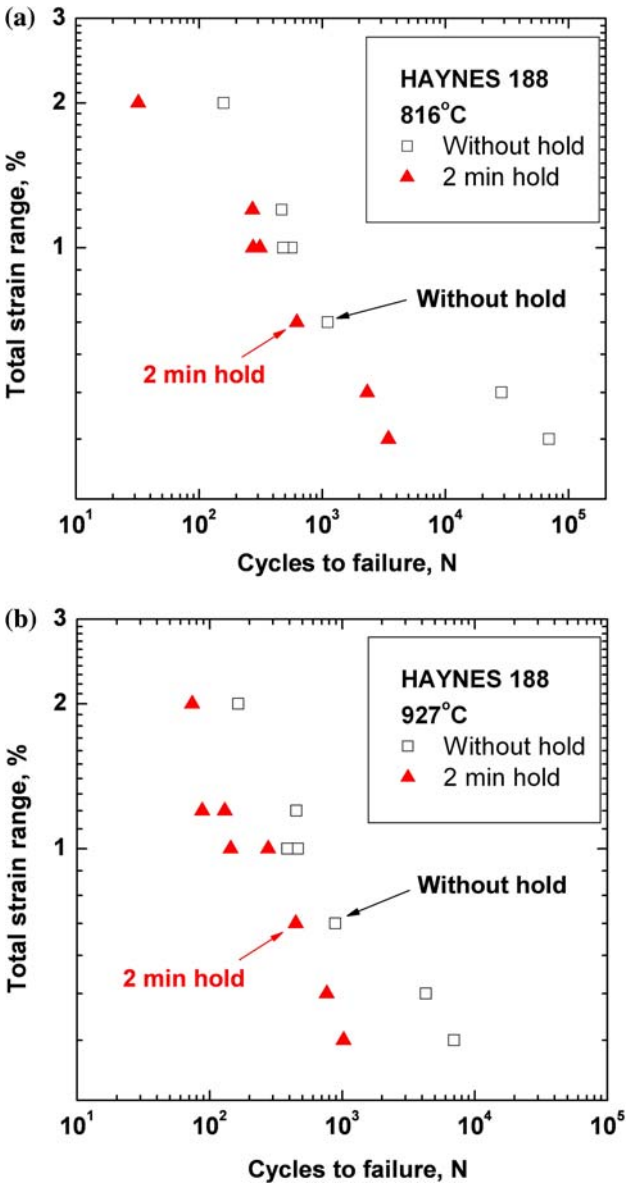

Fig. 7 Effect of 2-min-hold time on the LCF life at **a** 816 °C and **b** 927 °C

at high temperature, the cavities evolved along the grain boundaries can be thought of as a source of intergranular crack initiation accompanying stress concentration. Thus, the creep damage would lead to a change in the fracture mode from transgranular to intergranular features. In addition, an intergranular crack propagation usually shows higher crack-growth rates than transgranular crack propagation, indicating time-dependent cracking [26, 27]. Consequently, the alloy exhibits a shorter fatigue life.

The oxidation damage could contribute to an observed reduction in the fatigue life, because it tends to accelerate the crack initiation and propagation processes of a fatigue crack. If the hold time is imposed, the influence of the oxidation damage can be more significant than that of the

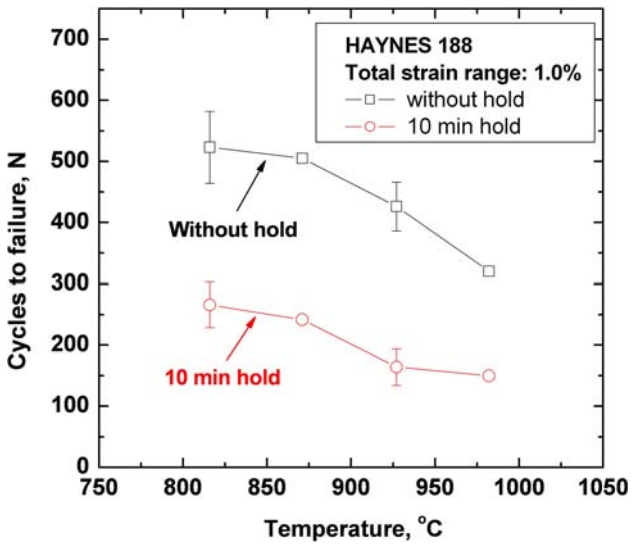

Fig. 8 Effects of temperature and 10-min-hold time on the LCF life. Error bars were used when more than one test were conducted

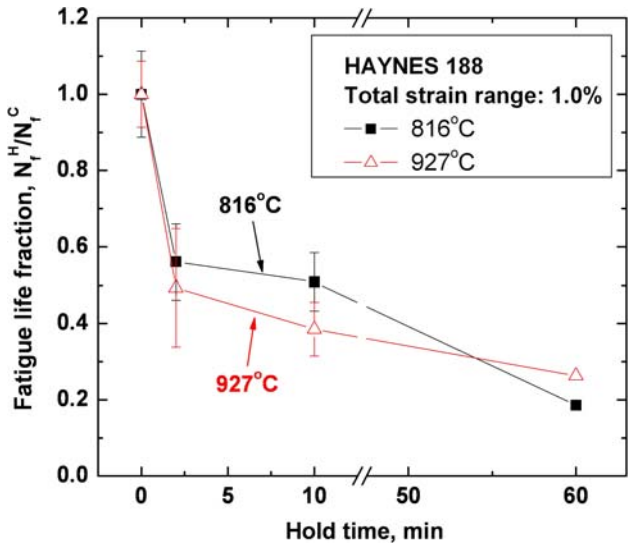

Fig. 9 Effect of hold time on the LCF life at the total strain range of 1.0%. Error bars were used when more than one test were conducted

LCF test without hold time. Longer time spent during the hold-time test would accelerate the formation of oxides along the grain boundaries that have high diffusivity path, resulting in oxidation-assisted intergranular crack growth. Thus, oxidation damage can also promote a substantial reduction of the fatigue life.

Crack-growth behavior

The FCG tests with various hold times were performed under a constant ΔK controlled mode at 816 and 927 °C. In order to investigate the cycle-dependent and/or time-dependent crack-growth behavior, the hold time was converted to frequency using the following equation:

$$v = 1/(t_c + t_h) \quad (3)$$

v is the cyclic frequency, t_c is the time for continuous fatigue cycling (which is 0.05 min in this study), and t_h is the hold time applied at the maximum stress-intensity factor. The cyclic-crack-growth rate, da/dN, and unit time-crack-growth rate, da/dt, are plotted in log–log scale as a function of the test frequency, respectively, in Fig. 10a and b. The cycle-dependent and time-dependent cracking regions are also indicated in Fig. 10. da/dN for cycle-dependent cracking line and da/dt for time-dependent cracking line were obtained from the crack-growth tests with zero hold time (i.e., continuous FCG test) and infinite hold time (i.e., creep-crack-growth test), respectively.

In Fig. 10a, the cyclic-crack-growth rate increased significantly with decreasing the test frequency at both

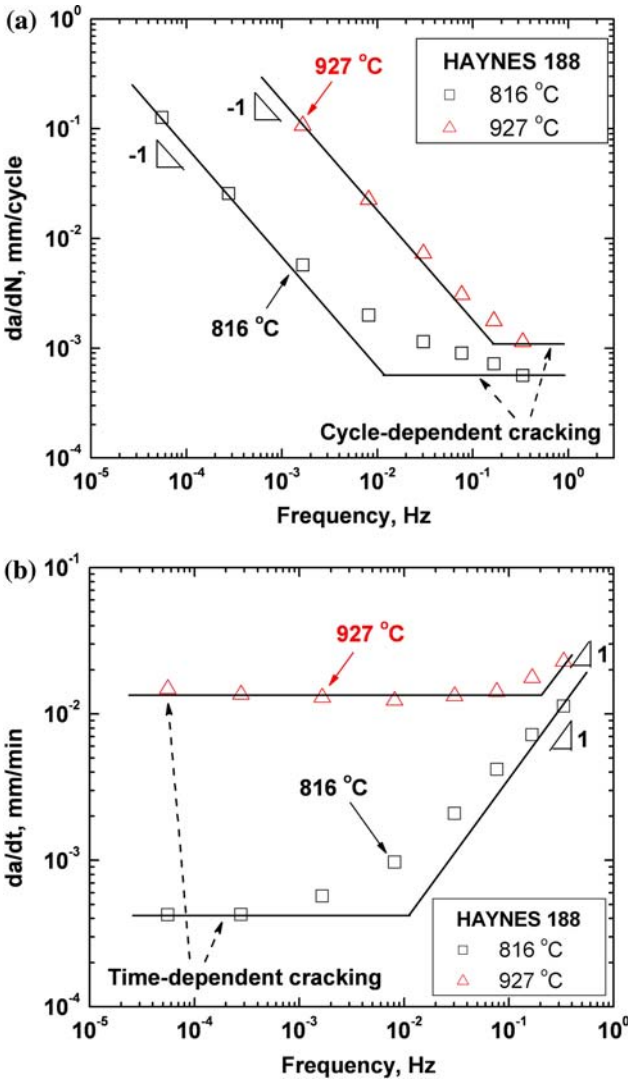

Fig. 10 Effect of frequency on **a** da/dN and **b** da/dt

temperatures. Especially, the slope of −1 in the log-log plot was observed in the region of low frequencies at both temperatures, indicating that the cyclic-crack-growth rate was inversely proportional to frequency. The longer hold time is applied, the greater increase of the crack length per cycle is obtained. Higher temperature resulted in faster cyclic-crack-growth rate at a given frequency. In Fig. 10b, it was found that the unit-time crack-growth rate increased considerably with increasing the test temperature. It is noted that the difference of crack-growth rate increases with decreasing the test frequency. It means that time-dependent cracking behavior became more significant at 927 °C than 816 °C. As a result, the time-dependent cracking region at 927 °C is observed earlier than that at 816 °C, as the frequency decreases. More specifically, the crack-growth behavior at 816 °C was dependent on time at frequencies below about 0.00028 Hz and on both cycle and time at frequencies above about 0.00028 Hz. On the other hand, the time-dependent behavior at 927 °C was observed at frequencies below about 0.08 Hz, and the crack-growth rate was dependent on both cycle and time at frequencies above about 0.08 Hz.

Cycle-dependent and time-dependent crack-growth behaviors are associated with the size of the fatigue-damage zone and creep-damage zone. The fatigue-zone size is a function of K. Under a constant ΔK controlled mode, the fatigue-zone size will maintain constant. On the other hand, the creep-damage zone size at the crack tip is dependent on the test temperature and hold time. As the temperature is higher and/or hold time is longer, a larger creep-damage zone size will be developed. Therefore, as the temperature and hold time increases, the creep-damage zone size grows larger than the fatigue-damage zone size, resulting in the time-dependent cracking behavior.

Fractography

The fracture of specimens subjected to the cyclic deformation generally involves two successive stages. Fatigue cracks first initiate and then propagate. In order to determine the crack initiation and propagation modes, the fracture surfaces of the failed specimen were carefully examined using SEM. Figure 11 shows the fracture surface of the sample subjected to only fatigue loading at 816 °C with total strain range of 0.7%. The typical fractographs that experience the transgranular crack initiation was observed. Figure 12 presents the intergranular crack initiation for the LCF test with 2-min-hold time at 927 °C with total strain range of 1.2%. A lot of secondary cracks along the grain boundaries were observed near the surface of the sample.

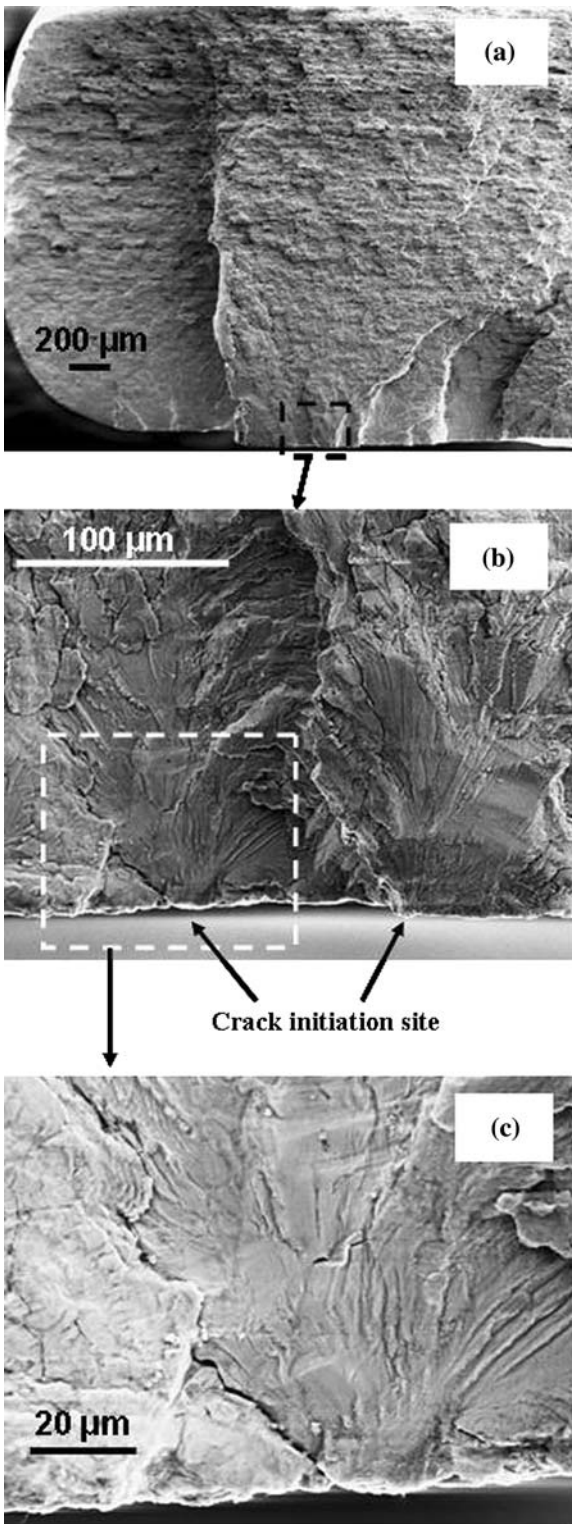

Fig. 11 SEM micrographs of the fracture surfaces. The test was conducted at 816 °C with total strain range of 0.7% and zero-hold time. **a** The entire fracture surface with low magnification; **b** higher magnification of the box area in (**a**) showing the multiple crack initiation sites; **c** higher magnification of the box area in (**b**) showing transgranular crack initiation

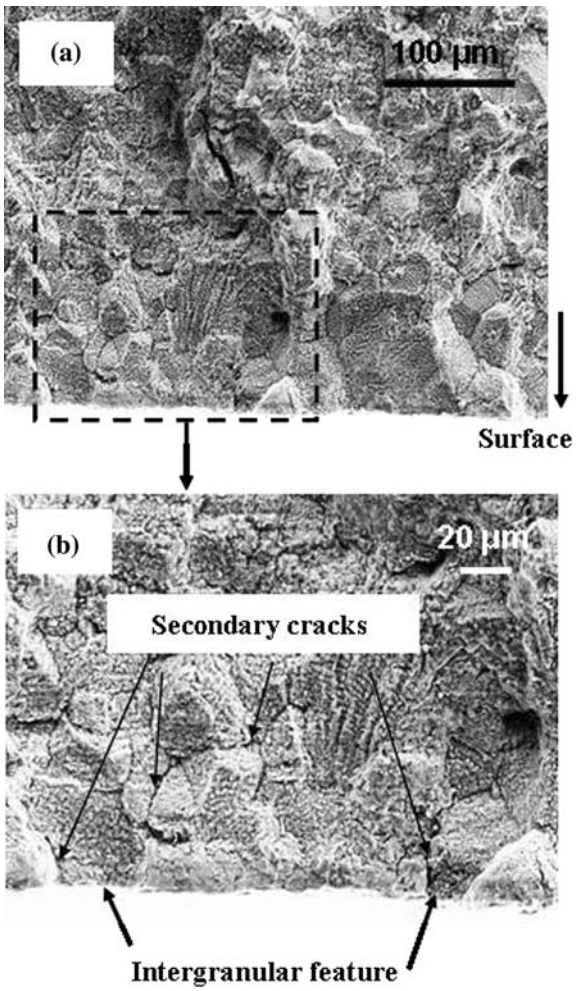

Fig. 12 SEM micrographs of the fracture surfaces. The test was conducted at 927 °C with total strain range of 1.2% and 2-min-hold time. **a** Intergranular crack-initiation region; **b** higher magnification of the box area in (**a**) showing the intergranular crack initiation site accompanying the secondary cracks

Figure 13a shows the fracture surface for the LCF test without hold time at 816 °C and total strain range of 1%. Clear fatigue striations were observed in all the fractured surfaces. A fatigue crack propagated in a transgranular mode. When the 2-min-hold time was introduced at the same total strain range and temperature, a mixed transgranular/intergranular mode was examined, as shown in Fig. 13b. Secondary crackings were often seen, indicating that grain boundary cavitation was evolved. As the temperature increased from 816 to 927 °C, the crack-propagation mode changed from a mixed transgranular/intergranular mode to an intergranular mode, as presented in Fig. 13c.

Based on these observations, it is obvious that the test temperature and hold time are very important factors for determining crack initiation and propagation modes. When the temperature and hold time increase, the intergranular

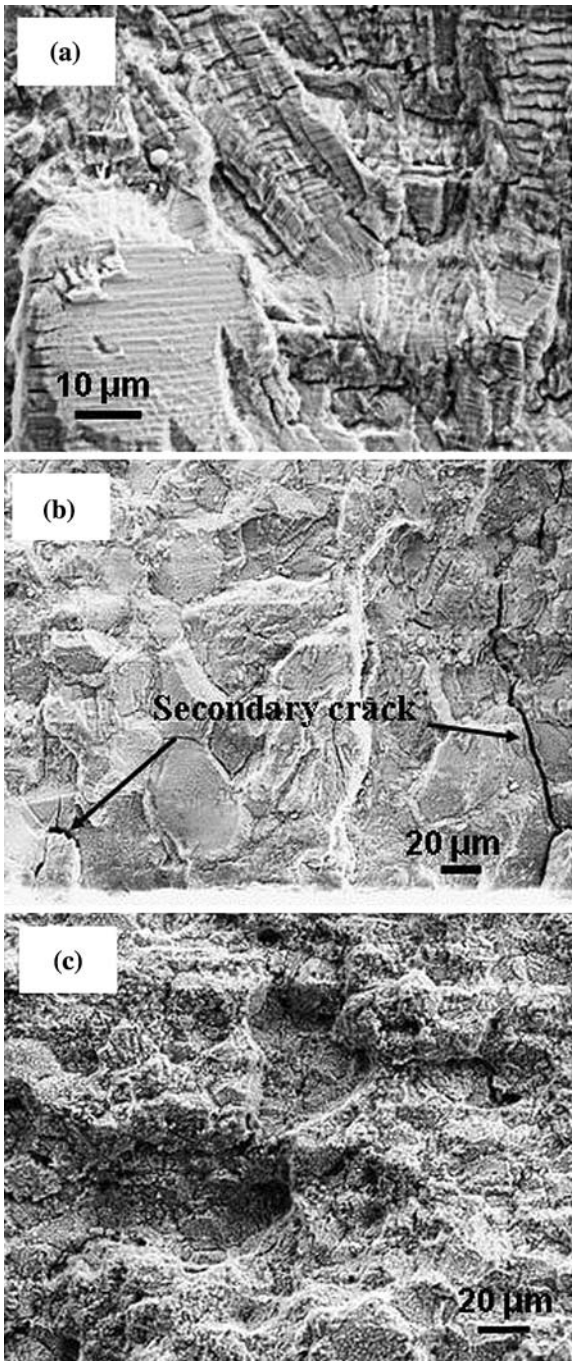

Fig. 13 SEM micrographs of the fracture surfaces. **a** Crack-propagation region (816 °C, a total strain range of 1.0%, zero-hold time); **b** crack-propagation region (816 °C, a total strain range of 1.0%, with 2-min-hold); **c** crack-propagation region (927 °C, a total strain range of 1.2%, 2-min-hold time)

cracking becomes the predominant crack initiation and propagation modes. The occurrence of the intergranular cracking may be explained as a consequence of two time-dependent damages, such as creep and oxidation. Creep strain that resulted from strain hold will induce the formation of voids at grain boundaries and expedite the

intergranular cracking. In addition, oxidation damage can promote intergranular crack initiation and propagation processes, because the brittle oxides can be formed easily along grain boundaries with high diffusivity path. From previous crack-growth studies with various hold times, it was found that the intergranular cracking path corresponded to the time-dependent cracking range and resulted in higher crack-growth rate [26, 27]. Therefore, an intergranular mode observed with increasing the temperature and hold time is thought of as a reflection of the reduction in the fatigue life.

Theoretical modeling: tensile-hysteresis-energy method

The hysteresis energy related to the plastic deformation can be used as a damage function of material subjected to cyclic loading, as proposed by Ostergren [28]. The hysteresis energy per cycle indicating the area of the stress–strain hysteresis loop is defined as the mechanical energy absorbed per unit volume during one cycle. Since the crack closure is occurred in the compressive portion of the cycle, only the deformation occurring in the tensile portion of the cycle is considered as the damage of a fatigue crack. Ostergren [28] proposed that the tensile-hysteresis energy per cycle, ΔU_{in}, can be approximated by the product of the inelastic strain range, $\Delta\varepsilon_{\text{in}}$, and the maximum tensile stress, σ_{T}:

$$\Delta U_{\text{in}} = \sigma_{\text{T}} \cdot \Delta\varepsilon_{\text{in}} \tag{4}$$

The calculated tensile-hysteresis energy using Eq. 4 tends to overestimate the experimentally measured value. If a numerical constant, $(1 - n')/(1 + n')$ used by Halford [29] is incorporated into Eq. 4, the estimated tensile-hysteresis energy is very close to the measured value.

$$\Delta U_{\text{in}} = \sigma_{\text{T}} \cdot \Delta\varepsilon_{\text{in}} \cdot [(1 - n')/(1 + n')] \tag{5}$$

where n' is the cyclic strain-hardening exponent.

By substituting the tensile-hysteresis energy for the inelastic strain component in the well-known Coffin-Manson equation with the form of $\Delta\varepsilon_{\text{in}} \cdot (N_{\text{f}})^{\beta} = C$, Eq. 6 is obtained.

$$\Delta U_{\text{in}} \cdot (N_{\text{f}})^{\beta} = C_1 \tag{6}$$

where N_{f} is the number of cycles to failure, and β and C_1 are the material constants.

Figure 14 shows the tensile-hysteresis energy as a function of cycles to failure using Eq. 6. The tensile-hysteresis energy had a good correlation with cycles to failure for the LCF tests without hold time, while the LCF tests with hold time did not follow a straight line.

A frequency-modified term was introduced into Eq. 6 to take account of the time-dependent damage with the hold time. Similar to the Coffin's frequency-modified equation

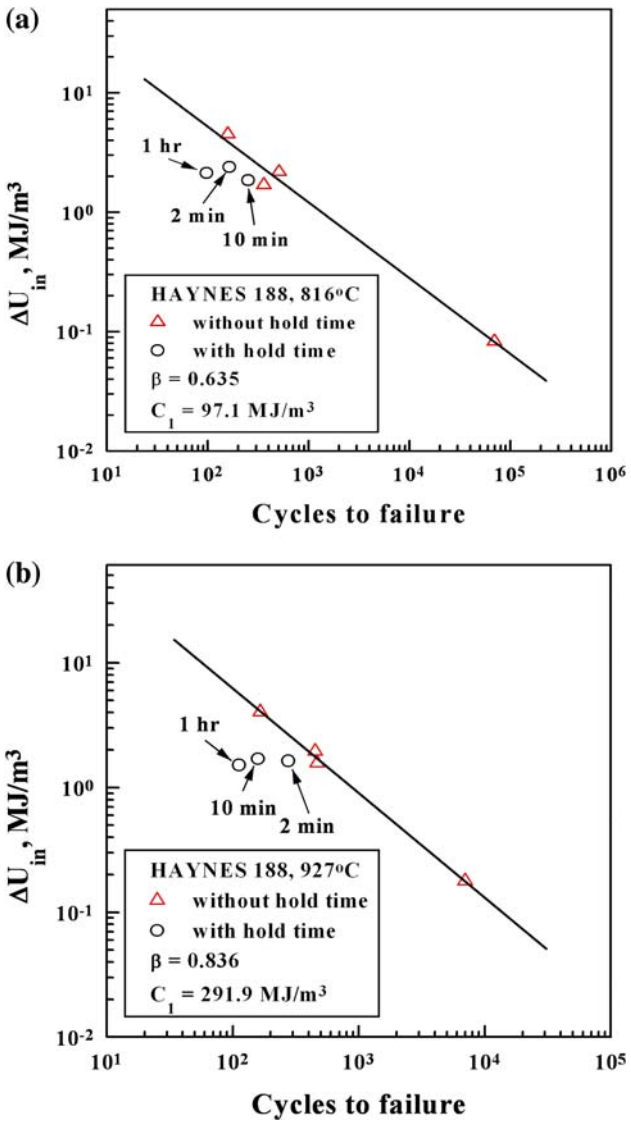

Fig. 14 The tensile-hysteresis energy as a function of cycles to failure with and without hold times at **a** 816 °C and **b** 927 °C

[30], the relationship between the frequency-modified tensile-hysteresis energy and cycles to failure can be expressed as

$$\Delta U_{\text{in}} \cdot \left(N_{\text{f}} \cdot v^{k-1}\right)^{\beta} = \text{C}_2 \tag{7}$$

where k and C_2 are material constants, and v is the cyclic frequency, which is defined as

$$v = 1/(t_{\text{c}} + t_{\text{h}}) \tag{8}$$

where t_{c} is the time for continuous cycling, and t_{h} the hold time imposed during the maximum tensile strain. The material constant, β, is the same as that in the tensile-hysteresis energy-life equation for LCF tests without the hold time at each temperature. In case of the cyclic frequency of 1 Hz, two constant terms in Eqs. 6 and 7, C_1 and C_2, should have the same value. The material

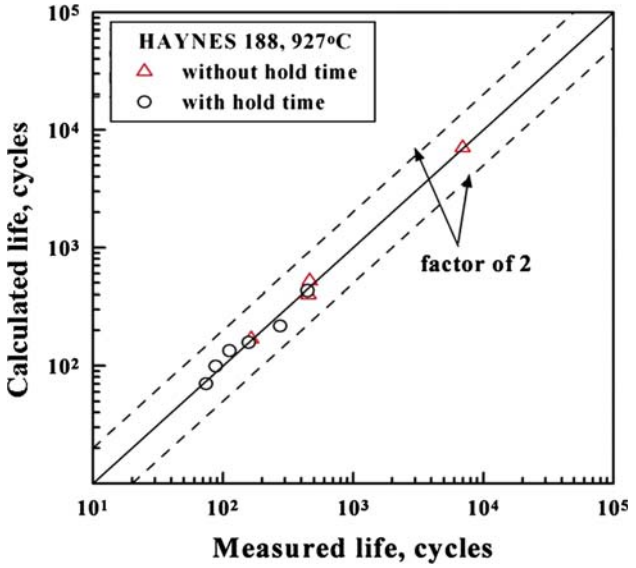

Fig. 15 Comparison of the measured fatigue life and calculated fatigue life using the frequency-modified hysteresis-energy method for the LCF tests with and without hold times at 927 °C

constants, k and C_2, can be determined by Eq. 7 through two tests with 2-min- and 10-min-hold times at the same total strain range of 1.0%.

Based on the frequency-modified tensile-hysteresis energy method, the fatigue lives of the 1-h-hold time at the total strain range of 1.0% and the 2-min-hold time at various total strain ranges were calculated by Eq. 7. Figure 15 shows the comparison between the calculated and measured fatigue lives. The calculated life had a good correlation with the measured life. Thus, Eq. 7 can be effectively used for correlating the fatigue life of the LCF tests.

Figure 16 shows a schematic of hysteresis loop for the test with tensile-hold time. The inelastic strain range, $\Delta\varepsilon_{in,}$ can be obtained by the summation of the plastic strain component, $\Delta\varepsilon_{pp}$ and the creep strain component, $\Delta\varepsilon_{cp}$.

$$\Delta\varepsilon_{in} = \Delta\varepsilon_{pp} + \Delta\varepsilon_{cp} \tag{9}$$

$\Delta\varepsilon_{pp}$ is determined from LCF test without the hold time, and $\Delta\varepsilon_{cp}$ is obtained by Eq. 10 from the stress-relaxation test.

$$\Delta\varepsilon_{cp} = \Delta\sigma_r/E \tag{10}$$

$\Delta\sigma_r$ is the relaxed stress during the hold time, and E is the modulus of elasticity.

With the introduction of hold time, Eq. 5 is written as Eq. 11.

$$\Delta U_{in} = \sigma_T \cdot \left(\Delta\varepsilon_{pp} + \Delta\varepsilon_{cp}\right) \cdot [(1-n')/(1+n')] \tag{11}$$

σ_T is the maximum tensile stress, which is determined from the LCF tests without the hold time.

Stress-relaxation tests were performed to obtain the tensile-hysteresis-energy parameter, $\Delta\varepsilon_{cp}$, required for the fatigue-life predictions with hold time and the results are

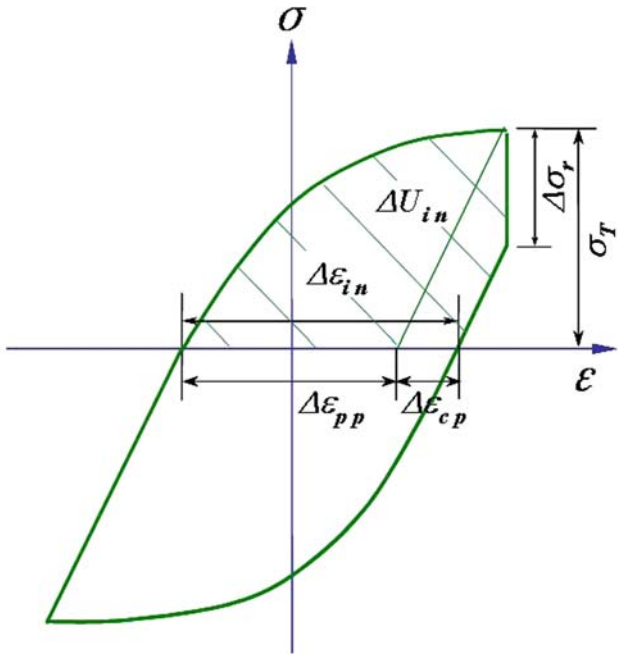

Fig. 16 Schematic of tensile-hysteresis energy with hold time

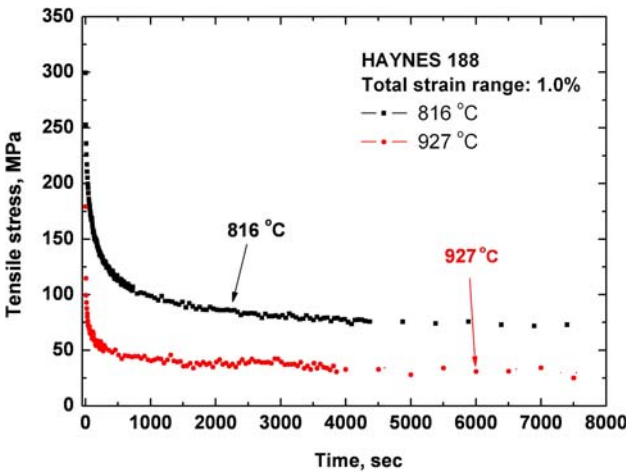

Fig. 17 Stress relaxation as a function of time in the stress-relaxation test at 816 °C and 927 °C

shown in Fig. 17. The samples were elongated with a monotonic tensile strain of 0.5%, and then the stress relaxation was monitored as a function of time at 816 and 927 °C. At both temperatures, the tensile stress decreased very rapidly during an initial 10-min-hold time. During the remaining portion of the hold time, however, the rate at which the stress relaxed was greatly reduced. It was found that the creep-strain rate decreased with increasing the hold time.

The creep-strain components ($\Delta\varepsilon_{cp}$) were obtained by Eq. 10 using the relaxed stress ($\Delta\sigma_r$) during several hold times of 2 min, 10 min, and 60 min from the

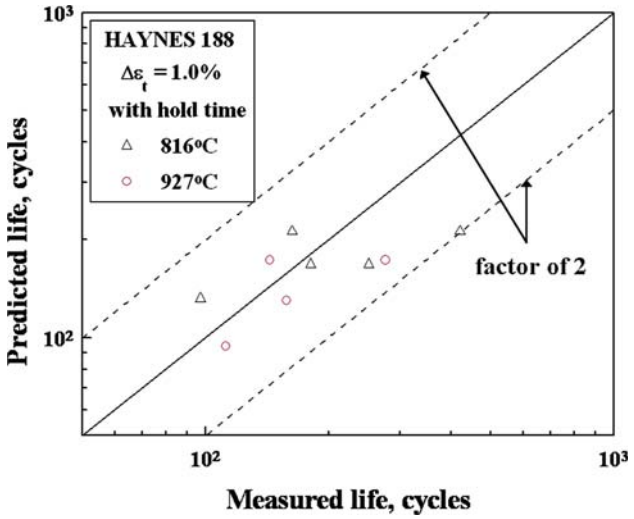

Fig. 18 Fatigue-life prediction using the frequency-modified hysteresis-energy method for the LCF tests with hold times from 2 to 60 min at 816 and 927 °C

stress-relaxation tests, and the tensile-hysteresis energy (ΔU_{in}) with these hold times was determined by Eq. 11. For the LCF tests with various hold times (e.g., 2-, 10-, and 60-min-hold time) and total strain range of 1% at 816 and 927 °C, the fatigue life was predicted by Eq. 7 without actually performing fatigue experiments, as presented in Fig. 18. A comparison of the predicted life and the measured one revealed a good correlation with a factor of 2.

In summary, a frequency-modified tensile-hysteresis energy method showed a good correlation between tensile-hysteresis energy and fatigue life for the LCF tests with and without hold time. Especially, this method can be considered as a useful way to predict the LCF life with various hold times at a given total strain range and temperature in that only one stress-relaxation test is required at the same conditions.

Conclusions

1. The cyclic-stress response curve of the HAYNES 188 alloy depended on the test temperature, the duration of hold time, and the imposed total strain range. The increase of the temperature and the introduction of hold time decreased the hardening rate and increased the softening rate. The hold-time effect increased with decreasing the total strain range.
2. The introduction of hold time at the maximum tensile strain was found to lead to a significant reduction in the fatigue life at all the total strain ranges from 0.4% to 2.0%.
3. Both cyclic-crack-growth rate and unit time-crack-growth rate considerably increased with increasing the temperature. The time-dependent cracking behavior at 927 °C was more significant than that at 816 °C.
4. The increase of the test temperature and/or the introduction of hold time tend to change the fracture mode from a transgranular to mixed transgranular/intergranular mode, and then to an intergranular mode.
5. A theoretical method based on the tensile-hysteresis energy was developed to correlate the measured LCF life, and a good correlation between tensile-hysteresis energy and fatigue life was obtained for the LCF tests with and without hold time. The fatigue life with hold time was reasonably predicted within a factor of 2 using this method.

Acknowledgements This work is supported by the Solar Turbines, Inc., Haynes International, Inc., the Center for Materials Processing (CMP) at the University of Tennessee (UT), the U. S. Department of Energy's Advanced Turbine Systems Program, the National Science Foundation (NSF), under Grant No. DMI-9724476, the NSF Combined Research-Curriculum Development (CRCD) Programs, under EEC-9527527 and EEC-0203415, the Integrative Graduate Education and Research Training (IGERT) Program, under DGE-9987548, the International Materials Institutes (IMI) Program under DMR-0231320, and the Major Research Instrumentation (MRI) Program, under DMR-0421219, with Ms. M. Poats, and Drs. C.V. Hartesveldt, J. Giordan, D. Dutta, P.W. Jennings, L.S. Goldberg, L. Clesceri, C. Huber, and C.E. Bouldin as contract monitors.

References

1. Haynes online literature, No. H-3001, Haynes 188 alloy product brochure: http://www.haynesintl.com/pdf/h3001.pdf
2. Merrick HF (1974) Metall Trans 5:891
3. Fournier D, Pineau A (1977) Metall Trans A 8:1095
4. Burke MA, Beck CG (1984) Metall Trans A 15:661
5. Antolovich SD, Liu S, Baur R (1981) Metall Trans A 12:473
6. Bashir S, Taupin P, Antolovich SD (1979) Metall Trans A 10:1481
7. McMahon CJ, Coffin LF (1970) Metall Trans 1:3443
8. Lerch BA, Jayaraman N, Antolovich SD (1984) Mater Sci Eng 66:151
9. Rao KBS, Schiffers H, Schuster H et al (1988) Metall Trans A 19:359
10. Berling JT, Conway JB (1970) Metall Trans 1:805
11. Lord DC, Coffin LF (1973) Metall Trans 4:1647
12. Chen W, Wahi RP (1998) In: Proceedings of the 6th Liege conference on materials for advanced power engineering. Belgium, p 1069
13. Klarstrom DL, Lai GY (1988) In: Superalloys, p 585
14. Mondel A, Lang KH, Lohe D et al (1997) Mater Sci Eng A 234:715
15. Rao KBS, Castelli MG, Allen GP et al (1997) Metall Mater Trans A 28:347
16. Rao KBS, Castelli MG, Ellis JR (1995) Scripta Mater 33:1005
17. Chen LJ, Liaw PK, He YH et al (2001) Scripta Mater 44:859
18. Lee SY, Lu YL, Liaw PK et al (2009) Mater Sci Eng A 504:64
19. Tawancy HM, Klarstrom DL, Rothman MF (1984) J Metals 36:58
20. ASTM Standard E647-99: Standard Test Method for Measurement of Fatigue Crack-Growth Rates, 2000 Annual Book of ASTM Standards, vol 03.01, p 591

21. Johnson HH (1965) Mater Res Stand 5:442
22. Liaw PK, Leax TR, Williams RS et al (1982) Metall Trans 13:1607
23. Vecchio KS, Fitzpatrick MD, Klarstrom D (1995) Metall Mater Trans A 26:673
24. Chen LJ, Liaw PK, Wang H et al (2004) Mech Mater 36:85
25. Lu YL, Chen LJ, Wang GY et al (2005) Mater Sci Eng A 409:282
26. Lu YL, Chen LJ, Liaw PK et al (2006) Mater Sci Eng A 429:1
27. Lee SY, Lu YL, Liaw PK et al (2008) Mech Time-Depend Mater 12:31
28. Ostergren WJ (1976) J Test Eval 4:327
29. Halford GR (1966) J Mater 1:3
30. Coffin LF (1954) Trans Am Soc Mech Eng 76:931